

RESEARCH

Open Access



Ventral posteromedial nucleus of the thalamus gates the spread of trigeminal neuropathic pain

Yu Du^{1,2}, Shi-Da Lin¹, Xue-Qing Wu², Bao-Yu Xue¹, Yi-La Ding², Jia-Hang Zhang¹, Bei Tan², Guo-Dong Lou³, Wei-Wei Hu^{1*}, Zhong Chen^{2*} and Shi-Hong Zhang^{1*}

Abstract

Background Widespread neuropathic pain usually affects a wide range of body areas and inflicts huge suffering on patients. However, little is known about how it happens and effective therapeutic interventions are lacking.

Methods Widespread neuropathic pain was induced by partial infraorbital nerve transection (p-IONX) and evaluated by measuring nociceptive thresholds. *In vivo/vitro* electrophysiology were used to evaluate neuronal activity. Virus tracing strategies, combined with optogenetics and chemogenetics, were used to clarify the role of remodeling circuit in widespread neuropathic pain.

Results We found that in mice receiving p-IONX, along with pain sensitization spreading from the orofacial area to distal body parts, glutamatergic neurons in the ventral posteromedial nucleus of the thalamus (VPM^{Glu}) were hyperactive and more responsive to stimulations applied to the hind paw or tail. Tracing experiments revealed that a remodeling was induced by p-IONX in the afferent circuitry of VPM^{Glu}, notably evidenced by more projections from glutamatergic neurons in the dorsal column nuclei (DCN^{Glu}). Moreover, VPM^{Glu} receiving afferents from the DCN extended projections further to glutamatergic neurons in the posterior insular cortex (pIC). Selective inhibition of the terminals of DCN^{Glu} in the VPM, the soma of VPM^{Glu} or the terminals of VPM^{Glu} in the pIC all alleviated trigeminal and widespread neuropathic pain.

Conclusion These results demonstrate that hyperactive VPM^{Glu} recruit new afferents from the DCN and relay the extra-cephalic input to the pIC after p-IONX, thus hold a key position in trigeminal neuropathic pain and its spreading. This study provides novel insights into the circuit mechanism and preclinical evidence for potential therapeutic targets of widespread neuropathic pain.

Keywords Trigeminal neuropathic pain, Widespread neuropathic pain, Afferent remodeling, Ventral posteromedial thalamic nucleus, Posterior insular cortex, Dorsal column nuclei

*Correspondence:
Wei-Wei Hu
huww@zju.edu.cn
Zhong Chen
chenzhong@zju.edu.cn
Shi-Hong Zhang
shzhang713@zju.edu.cn

¹Department of Pharmacology, Department of Anesthesiology of the Second Affiliated Hospital, Zhejiang University School of Medicine, Hangzhou 310058, China

²Key Laboratory of Neuropharmacology and Translational Medicine of Zhejiang Province, College of Pharmaceutical Sciences, Zhejiang Chinese Medical University, Hangzhou 310053, China

³Department of Pharmacy, Sir Run Run Shaw Hospital, Zhejiang University School of Medicine, Hangzhou 310016, China



Introduction

Widespread neuropathic pain is a chronic condition characterized by spontaneous and evoked pain in multiple body regions, usually resulting from peripheral nerve injury, but disproportionate in magnitude or duration to the typical neuropathic pain [1–3]. In clinical practice, it is frequently observed that damage to craniofacial nerves, notably the infraorbital and inferior alveolar nerves, precipitates a heightened sensitivity to pain beyond the orofacial area [4–6]. For instance, trigeminal neuropathic pain (TNP), a type of neuropathic pain originating from trigeminal nerve injury, primarily presents as unilateral orofacial pain [7]. However, it can extend beyond the trigeminal territory in a subset of patients to contralateral facial areas or even distal extremities with increased intensity and persistence, leading to more severe pain syndrome including anxiety and depression, both of which are inadequately managed by standard treatment with analgesics and antidepressants [8, 9]. Such phenomena imply that craniofacial nerve injuries, known for provoking severe pain in the orofacial region, predispose people to widespread neuropathic pain. Coincidentally, we previously reported that pain sensitization after partial infraorbital nerve transection (p-IONX) spreads from orofacial region to distal body parts, but that after partial sciatic nerve injury is restricted in the hind limb [10]. We also reported that spinal neuroinflammation contributes to the spreading process [6, 10, 11]. However, it is still unknown whether brain changes are involved in widespread neuropathic pain.

Accumulating studies have revealed that neural circuitry in the central nervous system (CNS) is undergoing remodeling in response to peripheral nerve injury [12, 13]. Anatomical and morphological changes, such as the restructuring of presynaptic axon terminals and postsynaptic dendritic spines due to primary afferent fiber transection or constriction, lead to functional modifications within neural circuitry [14, 15]. This remodeling, particularly the somatotopic remodeling, is strongly linked to the development of phantom limb sensations [16]. Moreover, it is found that thalamocortical reorganization develops after inferior alveolar nerve transection and contributes to the maintenance of extraterritorial pain [17]. In addition, transection of dorsal columns in macaque monkey results in expansion of receptive field from the face to the hand region of neurons in primary somatosensory cortex and ventroposterior nucleus of thalamus [17]. Further study identified that this expansion probably stems from remodeling in the brain stem but not intracortical or thalamocortical connections [18]. These findings indicate that peripheral nerve injury is able to cause circuitry remodeling in the brain and consequently may disturb pain sensation.

The sensory thalamus acts as an essential relay station in the pain transmission pathway, conveying sensory information from the secondary sensory neurons in the spinal cord and brain stem to the cortex, for instance, the somatosensory cortex, where the sensory and discriminative aspects of pain are processed [19]. The ventral posteromedial (VPM) and ventral posterolateral (VPL) thalamic nuclei, the two components of sensory thalamus, encode sensations from distinct body regions [20, 21]. The former predominantly processes orofacial sensory input from the trigeminal nuclei, while the latter primarily receives sensory information from the trunk and limbs via the dorsal column nuclei (DCN, comprising the gracile and cuneate nuclei) and the spinal dorsal horn [22, 23]. Under physiological conditions, these sensory pathways maintain a high degree of specificity and independence, a mechanism critical for the precise discrimination of the location and intensity of stimuli. The key position that the VPM holds in the trigeminothalamic pathway underscores its importance in pain and its management. Studies have indicated that the rhythmic burst firing of thalamic neurons may be involved in the development of chronic pain, and abnormal activity of VPM neurons are frequently observed in patients with neuropathic pain [24]. Moreover, deep brain stimulation (DBS) has been shown to effectively alleviate refractory facial pain [25]. Interestingly, few studies reported that after infraorbital nerve transection, VPM neurons exhibit responses to stimuli applied to the trunk or limbs, and the VPM starts to recruit afferents from the cuneate nucleus [26, 27]. However, whether and how these changes in the sensory thalamus contribute to the spread of neuropathic pain remain to be elucidated.

In this study, we reported that the glutamatergic neurons in the VPM (VPM^{Glu}) recruit more projections from the DCN after p-IONX. Selectively inhibiting this newly developed circuit of DCN-VPM significantly delayed and mitigated widespread pain sensitization. Moreover, selective inhibition of VPM^{Glu} and their projection terminals in the posterior insula cortex (pIC) alleviated both trigeminal and widespread pain sensitization. The study elucidates the circuit mechanism underlying the spread of TNP and highlights the potential value of VPM^{Glu} in the treatment of TNP with or without spread.

Methods

Briefly, all animal procedures were approved by the Zhejiang University Animal Experimentation Committee and were conducted in accordance with the National Institutes of Health Guide for the Care and Use of Laboratory Animals. Widespread neuropathic pain was induced by p-IONX and evaluated on D3-D28 postoperatively (PO) by measuring nociceptive thresholds to mechanical and heat stimulation in different body regions. Single-unit

and patch clamp recordings as well as fiber photometry were conducted to evaluate neuronal activity on D7 PO. Anterograde or retrograde virus tracing, combined with optogenetics and chemogenetics, was used from D1-D7 or D7-D14 PO to clarify the role of circuits in widespread neuropathic pain.

Animals

Adult (8–12 weeks old) male MRL/MPJ (MRL thereafter) and *Vglut2-Cre* mice were used in this study. Breeders were acquired from the Jackson Laboratory and SLAC Laboratory Animal, respectively, and propagated at Zhejiang University's Experimental Animal Center. Mice were group-housed (five per cage) under controlled humidity (45–65%), temperature (22–24 °C), and a 12-hour light/dark cycle (08:00 to 20:00 light period). Regular chew and clean water were available ad libitum. All procedures were in accordance with the guidelines of the International Association for the Study of Pain [28] and were approved by the Zhejiang University Animal Experimentation Committee. Efforts were made to minimize the animal use and suffering.

Partial infraorbital nerve transection surgery

The p-IONX surgery was performed as previously described [6]. In brief, under isoflurane anesthesia (4% for induction and 2% for maintenance), the mouth of the mouse was opened by pulling the lower and upper fore teeth with a rubber thread. Under the surgical microscope, a 2–2.5 mm incision was made from the gingival mucosa of the first molar on the left side to expose the deep branches of the ION. Approximately 1 mm of the nerve fibers was excised with a pair of microsurgical scissors and an absorbent gelatin sponge was placed on the wound. The nerve branches of mice in the sham group were exposed but left uninjured.

Delivery of virus and agents

Stereotaxic intracerebral injection was performed on a stereotaxic frame (RWD, China) under anesthesia induced with an intraperitoneal (i.p.) injection of sodium pentobarbital (50 mg/kg). The body temperature of the mouse was kept at 36 °C throughout the procedure using a heating pad. Small craniotomies were made over the target nuclei either for immediate viral delivery or implantation of guide cannula [outer diameter (o.d.): 0.41 mm; RWD, China] or chronic fiber optic cannula [core diameter: 200 µm, 0.22 mm numerical aperture (NA); Newdoon, China]. The coordinates of target nuclei relative to bregma were as follows according to the Paxinos and Franklin (2001) atlas: right VPM (AP: -1.7 mm, ML: -1.6 mm, DV: 3.5 mm), right pIC (AP: 0.2 mm, ML: -3.4 mm, DV: 3.9 mm), and left DCN (AP: -7.7 mm, ML: 1.1 mm, DV: -4.2 mm). The cannulas were held in place

by dental acrylic and the patency was maintained with occlusion stylets. For virus injection, a thin glass capillary connected to a 1 µl microsyringe mounted on a micro-pump (World Precision Instruments, USA, WPI) was slowly lowered to the target nuclei. Virus at a total volume of 100–200 nl was delivered at a flow rate of 40 nl/min. The glass capillary was left in place for an additional 5 min after injection to allow the diffusion of virus particles and minimize the reflux along the injection track. The sites of cannula placement or viral expression were histochemically confirmed on cryogenic brain sections at the end of all experiments. The core of viral expression should be within the target nuclei according to the brain atlas and be matched with the cannula tips. Animals displaying incorrect sites were excluded from all analysis.

Anterograde tracing. Virus pAAV-CaMKII α -hChR2(H134R)-EYFP (AAV-CaMKII α -ChR2, 1.7×10^{13} vg/ml, OBIO, China; 100 nl) or Cre-dependent virus AAV-CAG-FLEX-ArchT-GFP (2.14×10^{12} vg/ml, OBIO; 100 nl) was injected into the DCN of MRL or *Vglut2-Cre* mice. Three weeks later, mice were transcardially perfused under deep anesthesia with pentobarbital, and 30 µm brain slices were prepared for tracing the EYFP signal. For anterograde trans-monosynaptic tracing, helper virus rAAV1/2-DIO-TK-GFP (AAV-DIO-TK-GFP, 2×10^{13} vg/ml, BrainVTA, China; 100 nl) was injected into the VPM of *Vglut2-Cre* mice and H129 Δ TK-mCherry (3×10^{11} vg/ml, BrainVTA; 100 nl) was injected into the same place three weeks later. Seven days later, mice were perfused, and brain slices were prepared for tracing the mCherry signal.

Retrograde monosynaptic tracing. A mix of helper viruses that contain rAAV-EF1 α -DIO-His-EGFP-2 α -TVA-WPRE-pA (AAV-DIO-TVA-EGFP, 3.77×10^{12} vg/ml, BrainVTA) and rAAV-EF1 α -DIO-RVG-WPRE-pA (AAV-DIO-RVG, 3.43×10^{12} vg/ml, BrainVTA; 1:1, 100 nl) was injected into the VPM or pIC of *Vglut2-Cre* mice. Three weeks later, RV-EnvA- Δ G-DsRed (3.43×10^{12} vg/ml, BrainVTA; 100 nl) was injected into the same sites. Seven days after the last injection, mice were perfused, and brain slices were prepared for tracing the DsRed signal.

Triple-loop tracing strategy. Helper viruses that contain rAAV-EF1 α -DIO-His-mcherry-2 α -TVA-WPRE-pA (AAV-DIO-TVA-mCherry, 5.33×10^{12} vg/ml, BrainVTA) and rAAV-EF1 α -DIO-RVG-WPRE-pA (AAV-DIO-RVG, 3.11×10^{12} vg/ml, BrainVTA; 1:1, 100 nl) were injected into the VPM of *Vglut2-Cre* mice. Three weeks later, RV-EnvA- Δ G-EGFP (2.00×10^{12} vg/ml, BrainVTA; 100 nl) was injected into the pIC. Seven days after the last injection, mice were perfused, and brain slices were prepared for tracing the DsRed signal.

Tracing strategy for whole-cell patch-clamp recording. rAAV-Ef1 α -DIO-EGFP-WPRE-pA (AAV-DIO-GFP,

1.95×10^{12} vg/ml, OBIO; 200 nl) and rAAV-Ef1 α -DIO-hChR2-mCherry-WPRE-pA (AAV-DIO-ChR2-mCherry, 1.63×10^{13} vg/ml, OBIO; 200 nl) was injected into the VPM and DCN of *Vglut2-Cre* mice respectively. Mice were perfused at least three weeks later, and brain slices were prepared for patch-clamp recording.

Chemogenetic inhibition. Virus pAAV-CaMKII α -hM4D(Gi)-mCherry-3xFlag-WPRE (AAV-CaMKII α -hM4D(Gi)-mCherry, 1.26×10^{13} vg/ml, OBIO; 200 nl) was injected into the VPM or DCN of MRL mice. Four weeks later, clozapine-N-oxide (CNO; Abcam, ab141704, UK) was administered intraperitoneally (0.1 mg/kg), or via a cannula (30 μ g) implanted in the VPM or pIC to regulate neurons or neural circuits.

Fiber photometry. Virus AAV2/8-mCaMKII α -GCaMP6s-WPRE-pA-EYFP (AAV-CaMKII α -GCaMP6s-EYFP, 2.82×10^{12} vg/ml, Taitool, China; 200 nl) was injected into the VPM of MRL mice. Four weeks later, the calcium signal in response to noxious stimulation of the tail was recorded by an optical fiber.

Behavioral assessment

All behavioral tests were conducted during the light phase (from 9 am to 5 pm). Mice were habituated in the testing room for at least 30 min before the test. Examiners were blinded to the groups of mice. The testing room was sound-proof and the illumination intensity was maintained at 80 lx with temperature at 24–26 °C. After each trial, the mice were put back into their home cages and the experimental apparatus was cleaned with 75% alcohol to eliminate the odor that may affect animal behavior. Evoked pain-like behaviors were assessed on different days.

Evoked pain-like behavior test of face. To test pain-like behaviors evoked by stimulation of the left vibrissal pad, the mouse was placed in a small cage made with metal mesh ceiling and wood bottom (10 \times 5 \times 5 cm [3]). Face-scratching is a manifestation of pain behavior in mice, referring to unilateral or bilateral scratching with the forepaw of the area innervated by the trigeminal nerve [29]. The number of face-scratching was counted for 5 min immediately after a 1.0 g von Frey hair stimulation. Noxious thermal stimulation was supplied by a laser pulse. The laser with a pulse width of 150 ms generated by an infrared diode laser machine (LYPE, China) was shot at the left vibrissal pad with the guidance of a red aiming beam. Evoked pain-like behaviors included scratching the vibrissal pad, shaking head or turning around the body. The laser intensity (A) was started from 15 A and incremented by 1 A. Each intensity was tested 3 times with an interval of at least 5 min. The threshold was defined as the intensity that induced pain-like behaviors at least 2 times out of 3 trials [6].

Evoked pain-like behavior test of hind paw. To test the pain-like behaviors evoked by stimulation of the hind paw, the mouse was placed in a plastic cylinder (height of 9 cm and diameter of 8 cm) with metal mesh bottom. Mechanical stimulation was applied to the plantar surface of the left hind paw by a set of von Frey hairs (North Coast Medical, Gilroy, CA) numbered 1–9 with bending force 0.008, 0.02, 0.03, 0.07, 0.16, 0.4, 0.6, 1.0 and 1.4 g, respectively. The test was started from hair No.5 (0.16 g) and progressed according to an up-down method. Each test constituted a constant number of five stimuli with an interval of at least 5 min. Each stimulus lasted about 2 s. A sharp withdrawal or an immediate flinch of the hind paw indicated a positive response. The final number of von Frey hair was determined by adding 0.5 to the number of the fifth test if responses were evoked or reducing 0.5 if not. The paw withdrawal threshold (PWT) to mechanical stimulation was calculated by the equation: PWT force = $10(x * F + B)$ (F is the final number of von Frey hair, $x = 0.240$, $B = -2.00$) [30]. Noxious thermal stimulation was supplied by a laser pulse with a wave width of 200 ms that was shot at the plantar surface of the left hind paw. The laser intensity was increased by 1 A step, and each intensity was tried 3 times with an interval of at least 5 min. The PWT was defined as the intensity that evoked withdrawal responses at least 2 times out of 3 trials.

Evoked pain-like behavior test of tail. The mechanical threshold of tail was detected by von Frey test for the hind paw as above described. A sharp swing or an immediate flinch of the tail indicated a positive response. Hargreaves test was used for the evaluation of thermal nociception. A radiant heat source (Ugo Basile, Italy) with an intensity of 20 W was positioned underneath the glass bottom and aimed at the middle segment of tail. The withdrawal latency was recorded automatically. Minimum and maximum cutoffs were assigned at 1 and 20 s, respectively. The trial was repeated at a 15 min interval, and the average of two trials was taken into analysis.

Conditioned place preference (CPP) test. The CPP test is conventionally used to evaluate the affective responses to a particular treatment. However, based on the hypothesis that pain relief is rewarding, a pain-alleviating treatment can induce preference for the paired place in rodents [31]. Therefore, here we used the CPP test to examine whether manipulation of neuronal activity affects the affective status and/or spontaneous ongoing pain before and on D14 PO, respectively. The CPP test was conducted in a three-chamber apparatus that consists of two compartments of equal size (45 \times 40 \times 35 cm [3]) joined by a tunnel (40 \times 9 \times 35 cm [3]). Mice were first exposed to the pre-conditioning phase during which they were placed in the apparatus across 2 days and were allowed to explore the box freely for 30 min each day. Animal

behaviors on the second day were recorded by a digital video camera (Logitech, Switzerland) and the data in the last 15 min were analyzed by the ANY maze software to verify the absence of preference to any chamber. Animals spending more than 80% (720 s) or less than 20% (180 s) of the total time in any of the chambers were excluded from further testing. A four-day conditioning phase was then performed. Mice receiving CNO were placed into the box on one side for 30 min without access to other boxes on the third and the fifth days, while those receiving saline were placed into the other side on the fourth and the sixth days for 30 min. The post-conditioning phase was performed on day 7. Mice were placed into the middle tunnel with free access to chambers on both sides and their movements in each chamber were recorded for 15 min. The time spent in either chamber was analyzed by the ANY-maze and compared with that in the pre-conditioning phase.

Immunohistochemistry and imaging

Mice were deeply anesthetized with pentobarbital (100 mg/kg, i.p.), and then perfused with ice-cold PBS followed by 4% PFA. Brains were removed and post-fixed overnight in the same fixative, then dehydrated by infiltration in 30% sucrose for 48 h at 4 °C. Coronal slices were cut using a cryostat (ThermoFisher Scientific, USA) at 30 µm thickness and stored at -80 °C. Fluorescent images were captured by a fluorescence microscope (Olympus, Japan). For immunofluorescence staining, the sections were incubated with blocking buffer (0.1% Triton X-100, 5% donkey serum in PBS) for 2 h at room temperature (RT), and then were treated with primary antibodies against CaMKII α (1:500, rabbit, Abcam, ab171095) or GABA (1:500, rabbit, Sigma, USA, A2052) at 4 °C for 24 h. After washing three times for 5 min with PBS, the sections were incubated with donkey anti-rabbit AlexaFluor 594 (1:1000, Abcam, ab150080) or donkey anti-mouse AlexaFluor 488 (1:1000, Abcam, ab150105) conjugated secondary antibody for 2 h at RT. After repeated washing, the sections were then covered with glass coverslips and images were captured by a laser confocal microscope (Leica, German).

Fiber photometry

An optic fiber (o.d.: 0.20 mm, 0.37 NA; Inper, China) placed in a ceramic ferrule was inserted into the VPM 3 weeks after AAV-CaMKII α -GCaMP6s-EYFP injection. Mice were then allowed to recover for at least 1 week before subsequent test. The fiber photometry recording system (Thinkertech, China) used a dichroic mirror (MD498, Thorlabs, USA) to reflect a 488 nm laser (OBIS 488LS, Coherent, USA), which was focused with a 10x objective lens (0.3 NA; Olympus) and then coupled to an optical commutator (Doric Lenses, Canada). The

commutator and the implanted fiber were guided by a fiber cable (o.d.: 0.20 mm, 0.37 NA). GCaMP fluorescence was filtered using a GFP bandpass filter and collected using a photomultiplier tube (R3896, Hamamatsu, Japan). The amplifier converted the photomultiplier tube current output into a voltage signal that was further filtered by a low-pass filter (4 Hz cutoff; Brownlee, USA). The analog voltage signals were digitized at 500 Hz and recorded. Mice were anesthetized with isoflurane inhalation and mounted on a stereotaxic frame to ensure the head stable. Recording began after the mouse woke up from anesthesia. The fiber was connected to the fiber photometry setup and the baseline signals were recorded for 3 min before stimuli were applied. Pulse train electrical stimulation (automatic generator, 1 mA, 200 ms duration, 30 s intervals, 3 min duration/trial), pinch (clipping the tail for 10 s using a toothed plastic clip) or heat (immersing the tail into 55 °C hot water for 3 s duration) stimulation was applied on the tail. The calcium signals were then recorded continuously for 5 min. Photometry data were exported as MATLAB files for further analysis. We derived the values of fluorescence change ($\Delta F/F$) by calculating $(F-F_0)/F_0$, where F_0 is the averaged fluorescence over the 1 min baseline period before stimulation. $\Delta F/F$ value for each mouse was presented as heatmaps and the averaged values were presented in plots with the SEM indicated by a shaded area.

In vivo single-unit recordings

Mice were anesthetized with 20% urethane (1.4 g/kg, i.p.; Sigma-Aldrich, USA) and mounted on a stereotaxic frame. A small craniotomy was performed over the right VPM and VPL. The microelectrodes that consisted of 8 channels of wires (25 µm; AM-Systems, USA) with impedances of 1–2 M Ω were lowered into the target nuclei by a micromanipulator. Acquisition and analysis of data from single-unit recordings were conducted as previously described [32]. In short, signals were acquired by a multichannel acquisition system (Blackrock Microsystems, USA) with a sampling rate of 30 kHz and were high- and low-passed at 250 Hz and 7.5 kHz, respectively. The signals were analyzed by Offline Sorter (Plexon, USA) and NeuroExplorer 4.0 (NEX, USA). Putative glutamatergic neurons were identified by their wide spike waveform (full width at half maximum ≥ 0.30 ms) and sharp autocorrelation [33, 34]. The spontaneous and evoked firing of glutamatergic neurons in the right VPM (VPM^{Glu}) and VPL (VPL^{Glu}) were recorded 7 days after sham or p-IONX operation. The spontaneous firing was recorded for 3 min before recording the evoked firing by brush and pinch stimulation. Brush stimulus was applied by swapping the left vibrissal pad or hind paw for 60 s using a hairy brush. Pinch stimulus was applied by clipping the hind paw for 30 s using a toothed plastic clip.

Average firing rate before and during stimulation was quantified and compared. The response pattern of neuronal activity was classified as increased or decreased if the firing rates increased or decreased by more than 20% during stimulation compared with that before stimulation. Those that changed by no more than 20% were considered as no change.

Patch clamp electrophysiology

Brain slice preparation. Mice were deeply anesthetized with isoflurane and the brain was quickly removed to icy cold artificial cerebral spinal fluid (ACSF) oxygenated with 95% O₂ and 5% CO₂. Coronal slices (300 μm) that included the VPM and VPL were obtained using a vibratome (VT1000, Leica Instruments, Germany). The slices were then incubated for at least 30 min at 33 °C and another 1 h at RT in oxygenated ACSF. The brain slices were then transferred to a slice chamber and were continuously perfused with oxygenated ACSF at a rate of 3–4 ml/min before electrophysiological recordings at RT. For action potential recordings, the ACSF contained (in mM): 120 NaCl, 11 Dextrose, 2.5 KCl, 1.28 MgSO₄, 3.3 CaCl₂, 1 NaH₂PO₄, and 14.3 NaHCO₃, with pH at 7.4 and osmolality at 310.5 mOsm. For spontaneous post-synaptic current recordings, a low divalent ion ACSF containing (in mM): 125 NaCl, 3.5 KCl, 1.25 NaH₂PO₄, 0.5 MgCl₂, 26 NaHCO₃, 25 Dextrose, and 1 CaCl₂, with pH at 7.4 and osmolality at 310.5 mOsm was used.

Whole-cell patch-clamp recordings. Neurons of VPM and VPL in brain slices were visualized and recorded under an infrared differential interference contrast video microscopy mounted on an upright microscope (FN1, Nikon, Japan) that was equipped with a 340/0.80 water-immersion objective and a charge-coupled device camera (Clara-E, Andor Technology, UK). To record action potentials, pipettes with resistance of 5–10 MΩ and outer diameter of 1.5 mm were filled with a K⁺-based recording solution containing (in mM): 140 K-gluconate, 5 NaCl, 0.2 EGTA, 2 Mg-ATP and 10 HEPES. Stepped currents (0–200 pA, 10 pA per step) were injected into neurons to elicit action potentials. To record spontaneous excitatory and inhibitory post-synaptic currents (sEPSCs and sIPSCs), cesium-based recording solution containing (in mM): 100 CsCH₃SO₃, 20 KCl, 10 HEPES, 4 Mg-ATP, 0.3 Tris-GTP, 7 Tris₂-Phosphocreatine, and 3 QX-314) was used. The holding potential was –60 mV and +10 mV for recording sEPSCs and sIPSCs, respectively. Optical stimulation was performed using a blue laser (473 nm, 10 V, 20 ms, 5–10 Hz) through an optical fiber positioned 0.2 mm above the surface of the target brain region. The signals were amplified by the amplifier (EPC10, HEKA Instruments, Germany), and digitized at 10 kHz. The low-pass filter was set at 2.8 kHz. If the series resistance changed by more than 20% during the

recordings, the neuron was immediately abandoned. Data were further analyzed with MiniAnalysis Program (Synsoft Inc, USA) and Clampfit 10.7 software (Molecular Devices, USA) to provide spreadsheets for the generation of cumulative probability plots. The amplitude and inter-event interval of post-synaptic currents were collected.

Statistical analysis

All data are expressed as the mean ± SEM. The required sample sizes were estimated based on our experience and pilot experiments and Power analysis was used to justify the sample size. Statistical analysis was conducted by GraphPad Prism 8.0 (GraphPad Software, USA). Student's t-test was used to compare data of two groups. For comparisons among multiple groups, data were analyzed using one-way or two-way analysis of variance (ANOVA) with Tukey's or Bonferroni's post-hoc analyses. Significance levels are displayed as **p* < 0.05, ***p* < 0.01 and ****p* < 0.001.

Results

Neuronal activity of VPM^{Glu} is enhanced after p-IONX

On D3 PO and thereafter, mice in the p-IONX group exhibited a significant increase in scratching behavior and a notable decrease in the pain threshold to mechanical and heat stimulation applied to the vibrissal pad, compared with that before surgery (BL) and the sham group (Fig. 1A and B), suggesting the establishment of trigeminal neuropathic pain. From D7 PO, the p-IONX group demonstrated a substantial decrease in both mechanical and thermal pain thresholds in the hind paw (Fig. 1C). Furthermore, a reduction in pain thresholds was detected on the tail, together verifying that pain sensitization had spread from the territory of nerve injured to distal body areas (Fig. 1D).

We then explored whether the neuronal activity of sensory thalamus is changed following p-IONX. It has been proposed that neurons in the VPM and VPL are glutamatergic in rodents [35]. Whole-cell recordings revealed no change in resting membrane potentials in VPM and VPL neurons, but a significant reduction in rheobase (the lowest current intensity that evoked action potential firing) was detected alongside an elevated firing rate in response to stepwise current injection in VPM but not VPL neurons on D7 PO (Fig. 2A–D). Moreover, the amplitude and frequency of sEPSCs but not sIPSCs in VPM neurons were elevated significantly in the p-IONX group (Fig. 2E–G). In contrast, no differences in the postsynaptic currents were detected between the p-IONX and sham groups in VPL neurons (Fig. 2E, H–I).

In addition, the firing activity of VPM and VPL neurons was examined by *in vivo* single-unit recordings on D7 PO (Fig. 2J). The glutamatergic nature of recorded neurons was identified by the characteristic waveform

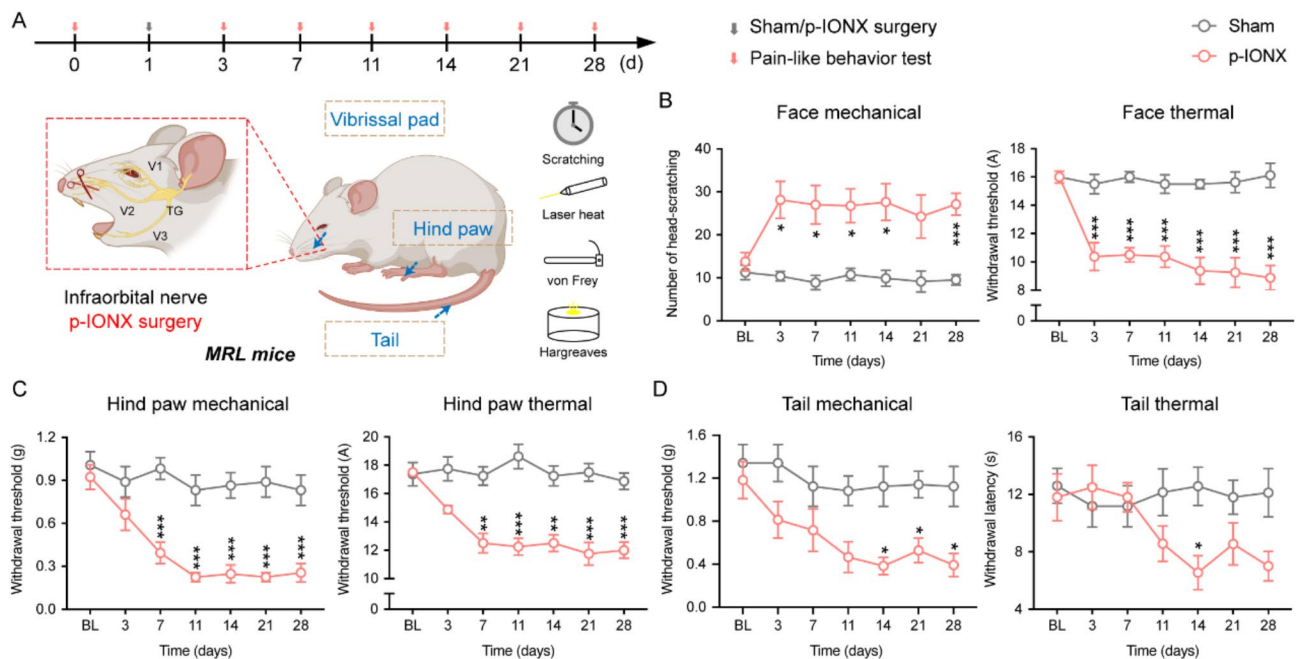


Fig. 1 p-IONX induces widespread neuropathic pain. **A**, Schedule of experimental procedure of pain-like behavior examination. **B**, Face mechanical and thermal thresholds were examined by face-scratching test and laser heat test. **C**, Hind paw mechanical and thermal thresholds were examined by von Frey test and laser heat test. **D**, Tail mechanical and thermal thresholds were examined by von Frey test and Hargreaves test. $n=8$ mice for each group. Significance was calculated by means of a two-way ANOVA with Bonferroni's post hoc test. * $p < 0.05$, ** $p < 0.01$ and *** $p < 0.001$, p-IONX versus sham

and the autocorrelation of neuronal discharge (Fig. 2K). It was revealed that the spontaneous firing of VPM^{Glu} rather than VPL^{Glu} was substantially increased in the p-IONX group (Fig. 2L). Moreover, we found that VPM^{Glu} and VPL^{Glu} responded to orofacial stimulation in three patterns: increased, decreased and no change. In sham-treated mice, the proportions of three response patterns in both VPL and VPM neurons were similar (Fig. 2M). The average firing frequency of VPM^{Glu} was increased by orofacial stimulation, whereas VPL^{Glu} did not show such shift (Fig. 2N-P). However, compared with the sham-treated group, VPM^{Glu} in p-IONX treated mice displayed a larger fraction (73.3% versus 26.7%) of the increased pattern in response to orofacial brush stimulation, leading to a significant elevation of the average firing frequency. By contrast, VPL^{Glu} exhibited no notable changes in response patterns as well as average firing frequency (Fig. 2M-P). These findings demonstrate that the excitability and excitatory synaptic transmission of glutamatergic neurons in the VPM but not VPL are markedly augmented following infraorbital nerve injury.

VPM^{Glu} are more responsive to sensory input from extra-cephalic regions following p-IONX

After demonstrating VPM^{Glu} , rather than VPL^{Glu} , were hyperactive following p-IONX, we then investigated whether VPM^{Glu} were involved in integrating sensory input from distant body regions beyond the orofacial

area. The response of VPM^{Glu} to innocuous (brush for 60 s) or noxious (pinch for 30 s) stimulation at the hind paw was examined on D7 PO (Fig. 3A-B). We found that although response pattern composition to brush was similar across groups, the p-IONX mice exhibited a substantially higher proportion of increased pattern in response to pinch (Fig. 3C). Meanwhile, VPM^{Glu} in the p-IONX group manifested a marked increase in firing frequency upon both types of stimulation, with a post-stimulus return to baseline levels gradually. By contrast, the sham group showed only a mild increase, significantly less pronounced than the p-IONX group (Fig. 3D-G). These results indicate that VPM^{Glu} in p-IONX mice respond with an amplified extent to stimulation of the hind paw, implying a remodeling of afferents.

Considering the responses of VPM^{Glu} to stimulation might be influenced by light anesthesia, which is necessary for single-unit recordings, we then examined the changes of calcium signals of VPM^{Glu} induced by noxious stimulation of the tail in awake animals (Fig. 3H-I). In the p-IONX group, the calcium signal in VPM^{Glu} showed a pronounced elevation in response to continuous 1-mA electrical shocks to the tail (Fig. 3J-M) or a 10 s of noxious pinch (Fig. 3N-O). In contrast, the sham group did not exhibit evident changes in calcium signal. Additionally, exposure of the mouse tail to hot water at 55 °C resulted in a substantial increase in calcium signal (Fig. 3P-Q). These data indicate that VPM^{Glu} in p-IONX-treated mice

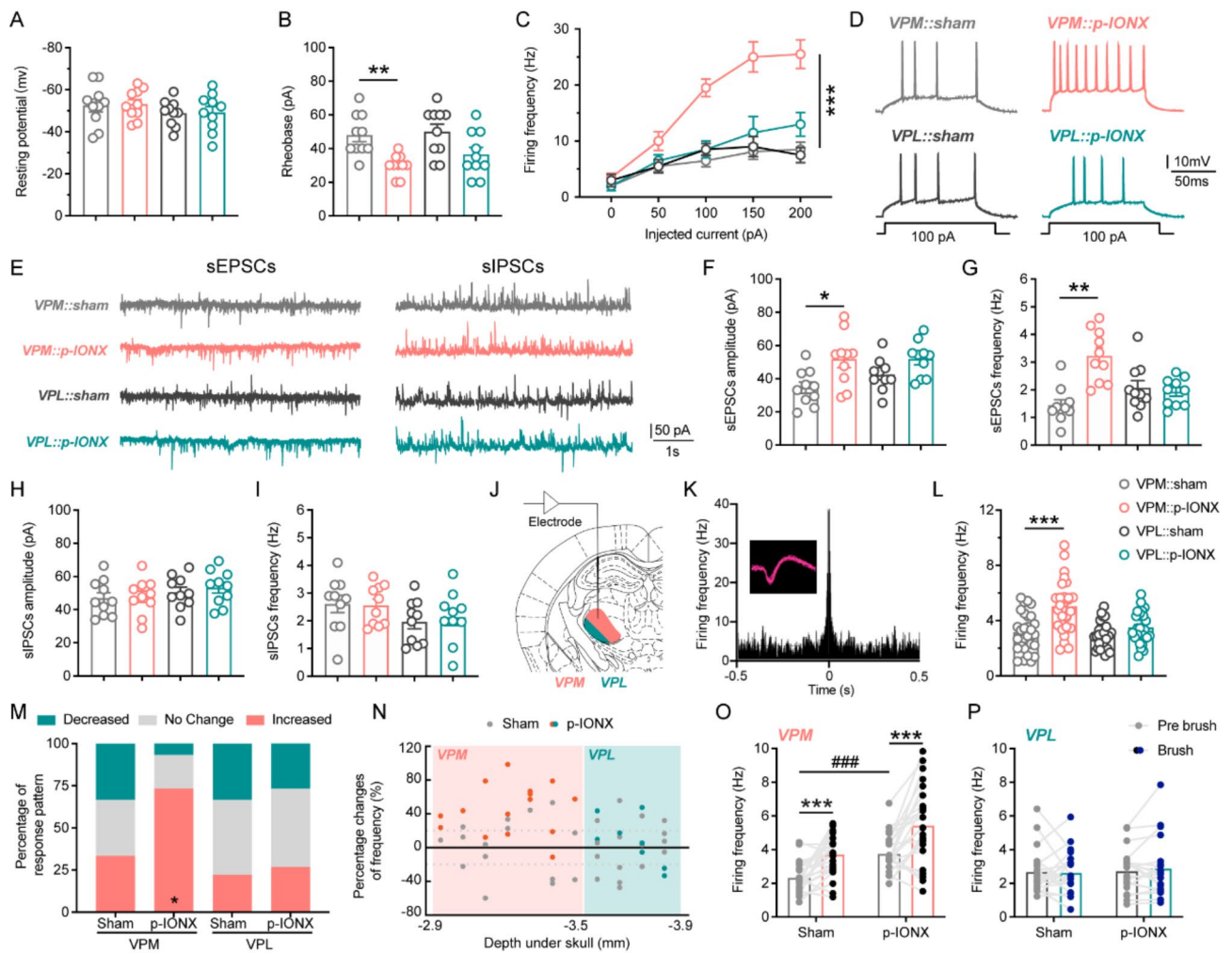


Fig. 2 VPM^{Glu}, but not VPL^{Glu}, are hyperactive following p-IONX. **A, B**, Resting potential (A) and rheobase (the lowest current that evoked action potential firing) (B) of VPM^{Glu} and VPL^{Glu} in sham- and p-IONX-treated mice on D7 PO. **C**, Firing frequency of action potential evoked by step-current injection. **D**, Sample traces of evoked action potentials. **E**, Sample traces of sEPSCs and sIPSCs recorded from VPM^{Glu} and VPL^{Glu} of sham- and p-IONX-treated mice on D7 PO. **F, G, H, I**, The amplitude, frequency of sEPSCs (F, G) and sIPSCs (H, I). *n* = 10 mice for A-I. **J**, Schematic of in vivo single-unit recordings in the VPM and VPL in sham- and p-IONX-treated mice on D7 PO. **K**, Autocorrelation and waveform (inset) of a representative glutamatergic neuron recorded by in vivo single-unit recordings. **L**, Mean frequency of spontaneous firing. *n* = 28 neurons from 10 mice/group. **M**, Proportion of VPM^{Glu} and VPL^{Glu} that show increased, decreased and no change pattern in response to orofacial brush stimulation. **N**, Changes in firing frequency of VPM^{Glu} and VPL^{Glu} and their corresponding depth relative to the brain surface in sham- and p-IONX- treated mice. Dashed lines indicate $\pm 20\%$, which are the boundary of different response pattern. **O, P**, Firing frequency of VPM^{Glu} (O) and VPL^{Glu} (P) before and during brush stimulation in sham- and p-IONX- treated mice. *n* = 24 from 10 mice for VPM^{Glu}, *n* = 20 from 7 mice for VPL^{Glu}, in both sham and p-IONX groups. Significance was calculated by means of a one-way ANOVA with Tukey's post hoc test in B, F, G, L, O; two-way ANOVA with Bonferroni's post hoc test in C, O. **p* < 0.05, ***p* < 0.01 and ****p* < 0.001, respectively, VPM::Sham versus VPM::p-IONX or brush versus pre; ###*p* < 0.001, p-IONX versus sham

are more responsive to noxious stimulation applied to the tail. Taken together, it was demonstrated that VPM^{Glu} are hyperactive after p-IONX and their responsiveness to peripheral stimulation extends beyond orofacial area, suggesting a possible involvement of VPM^{Glu} in widespread pain sensitization.

Inhibition of VPM^{Glu} or the circuit to the pIC alleviates widespread neuropathic pain and associated aversion

After confirming the hypersensitivity of VPM^{Glu} to stimulation of wide body regions after p-IONX, we further

explored the role of VPM^{Glu} in trigeminal and widespread neuropathic pain by chemogenetically inhibiting their activities. In mice receiving AAV-CaMKII α -hM4D(Gi)-mCherry injection into the VPM, CNO was administered i.p. daily for consecutive eight days during D7-D14 after p-IONX and the inhibition of neuronal activity by CNO was verified by patch clamp recordings (Fig. 4A-C). It was found that inhibition of VPM^{Glu} elevated mechanical and thermal pain thresholds of the face and hind paw (Fig. 4D-E). In addition, in the CPP test, p-IONX mice spent more time in the side paired with CNO than that

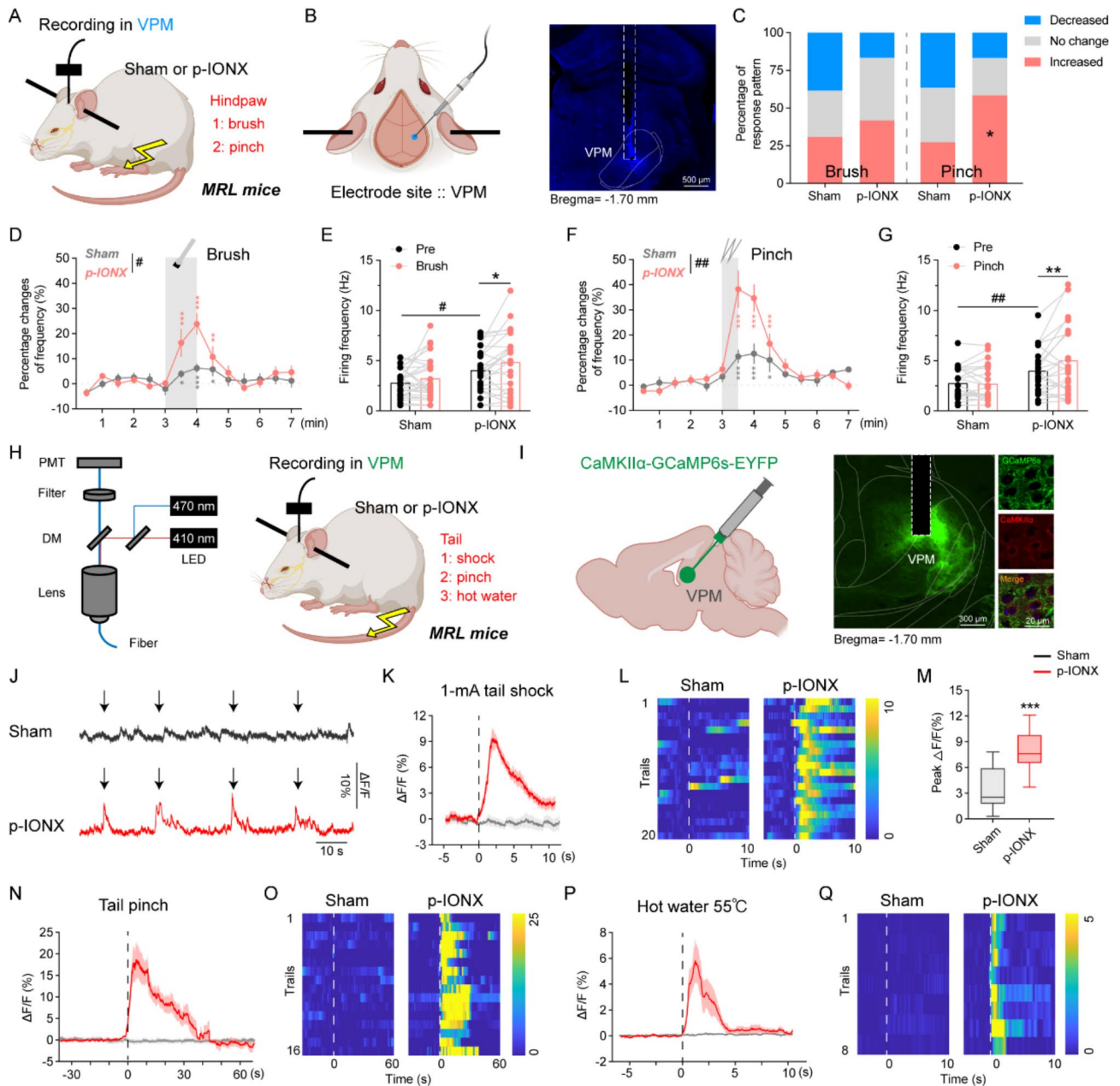


Fig. 3 VPM^{Glu} recruit somatosensory input from the hind paw and tail following p-IONX. **A**, Schematic drawing of single unit recordings of VPM^{Glu} and mechanical (brush or pinch) stimulation of the hind paw on D7 PO. **B**, Schematic (left) and photomicrograph (right) showing the recording site. **C**, Proportion of VPM^{Glu} that show increased, decreased and no change pattern in response to brush and pinch stimulation. **D**, Change of firing frequency pre-, during and post- brush. **E**, Mean firing frequency of VPM^{Glu} pre- and during brush. **F**, Change of firing frequency pre-, during and post- pinch. **G**, Mean firing frequency of VPM^{Glu} pre- and during pinch. *n* = 22–24 from 8 mice for D–G. **H**, Schematic drawing of the fiber photometry setup (left) and stimulation (shock, pinch or hot water) at the tail. **I**, Schematic of the AAV-CaMKIIα-GCaMP6s-EYFP injection in the VPM (left) and photomicrograph showing the colocalization of GCaMP6s-EYFP and CaMKIIα (right). **J**, Representative response of VPM^{Glu} to tail shock indicated by black arrow lines. **K**, **L**, **M**, Peri-event plot (K), heatmaps (L) and peak (M) of GCaMP6s ΔF/F peri-tail shock in sham- and p-IONX- treated mice. *n* = 20 from 5 mice for J–M. **N**, **O**, Peri-event plot (N) and heatmaps (O) of GCaMP6s ΔF/F peri-tail pinch. *n* = 16 from 4 mice for N–O. **P**, **Q**, Peri-event plot (P) and heatmaps (Q) of GCaMP6s ΔF/F peri-hot water stimulation. *n* = 8 from 4 mice for P–Q. Dashed lines indicate the start of stimulation. Significance was calculated by means of two-way ANOVA with Bonferroni’s post hoc test in D–G; student’s *t* test in M. **p* < 0.05 and ****p* < 0.001, respectively, brush or pinch versus pre, or sham versus p-IONX. #*p* < 0.05 and ##*p* < 0.01, p-IONX versus sham

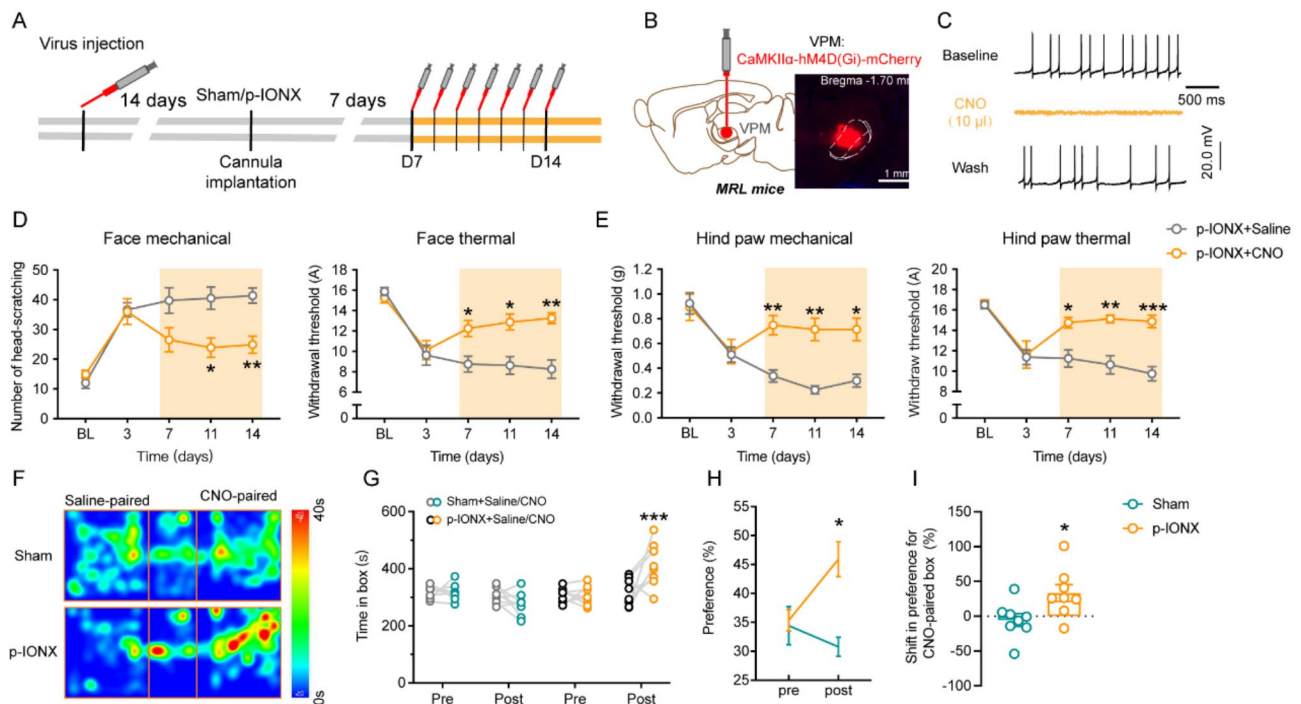


Fig. 4 Chemogenetic inhibition of VPM^{Glu} alleviates widespread neuropathic pain and associated aversion. **A**, Experimental design for chemogenetic inhibition of VPM^{Glu}. CNO was delivered daily during D7-D14 after p-IONX. **B**, Schematic of the AAV-CaMKIIα-hM4D(Gi)-mCherry injection in the VPM (left) and photomicrograph showing the injection site. **C**, Representative trace of action potentials induced by 20 pA current injection in an mCherry-labeled neuron in the VPM with or without CNO (Upper, baseline; Middle, CNO perfusion; Bottom, CNO washed out). **D, E**, Withdrawal thresholds to mechanical or thermal stimulation of the ipsilateral vibrissal pad (face) and hind paw before and after p-IONX. Yellow shadow areas indicate CNO perfusion period. **F**, Representative heat maps in the CPP test. **G, H, I**, Time spent by the mice in the saline- and CNO- paired boxes (G), preference (H) and shift preference (I) for the CNO-paired box in pre- and post-conditioning phases. *n* = 8 mice. Significance was calculated by means of two-way ANOVA with Bonferroni's post hoc test in D, E, H; student's *t* test in G, I. **p* < 0.05, ***p* < 0.01 and ****p* < 0.001, p-IONX + Saline versus p-IONX + CNO or post- versus pre- conditioning

in the saline-paired side (Fig. 4F-G). Moreover, the preference rate for the CNO-paired side significantly was increased in p-IONX mice (Fig. 4H-I). These results indicate that chemogenetic inhibition of VPM^{Glu} alleviated trigeminal and widespread neuropathic pain and/or associated aversive affect, demonstrating the pivotal role of VPM^{Glu} hyperactivity therein.

To further establish the role of VPM^{Glu} in widespread neuropathic pain, we probed the involvement of the circuit from VPM to pIC, which receives projections from multiple thalamic nuclei and is conventionally considered as a key area for pain perception [36, 37]. A mix of Cre-dependent helper virus AAV-DIO-TK-GFP and a genetically modified version of Herpes simplex virus type 1 strain 129 (H129ΔTK-mCherry) was injected into the VPM of *Vglut2-Cre* mice (Fig. 5A-B). Intense mCherry-labeled neurons were identified in the pIC and highly overlapped with CaMKIIα (Fig. 5C), indicating the pIC neurons receiving VPM^{Glu} projections are mainly glutamatergic. Then we inhibited the circuit of VPM^{Glu} to pIC by chemogenetics. AAV-CaMKIIα-hM4D(Gi)-mCherry was injected into the VPM and a cannula was implanted in the pIC, through which CNO was administered for consecutive eight days during D7-D14 after p-IONX to

selectively inhibit the projection terminals of VPM^{Glu} in the pIC (Fig. 5D-E). CNO treatment elevated the pain thresholds both on the face and hind paw (Fig. 5F-G). Moreover, in the CPP test, p-IONX mice showed preference to the CNO paired box (Fig. 5H-I). These results together suggest that inhibition of the circuit of VPM^{Glu}-pIC alleviates trigeminal and widespread neuropathic pain. Therefore, we concluded that VPM^{Glu} gate trigeminal neuropathic pain and its spread after p-IONX at least by the circuit to pIC.

VPM^{Glu} recruit more afferents from the DCN following p-IONX

After establishing the crucial role of VPM^{Glu} in widespread neuropathic pain, we used *Vglut2-Cre* mice expressing Cre recombinase in glutamatergic neurons to study whether p-IONX changed the afferent profile of VPM^{Glu}. We first confirmed that *Vglut2-Cre* mice developed widespread neuropathic pain after p-IONX (Fig. 6A-B), then Cre-dependent mixed helper viruses AAV-DIO-TVA-EGFP and AAV-DIO-RVG were injected into the VPM after p-IONX. Three weeks later, the rabies virus RV-EnvA-ΔG-DsRed was injected into the same site (Fig. 6C-D). The presence of helper viruses facilitated

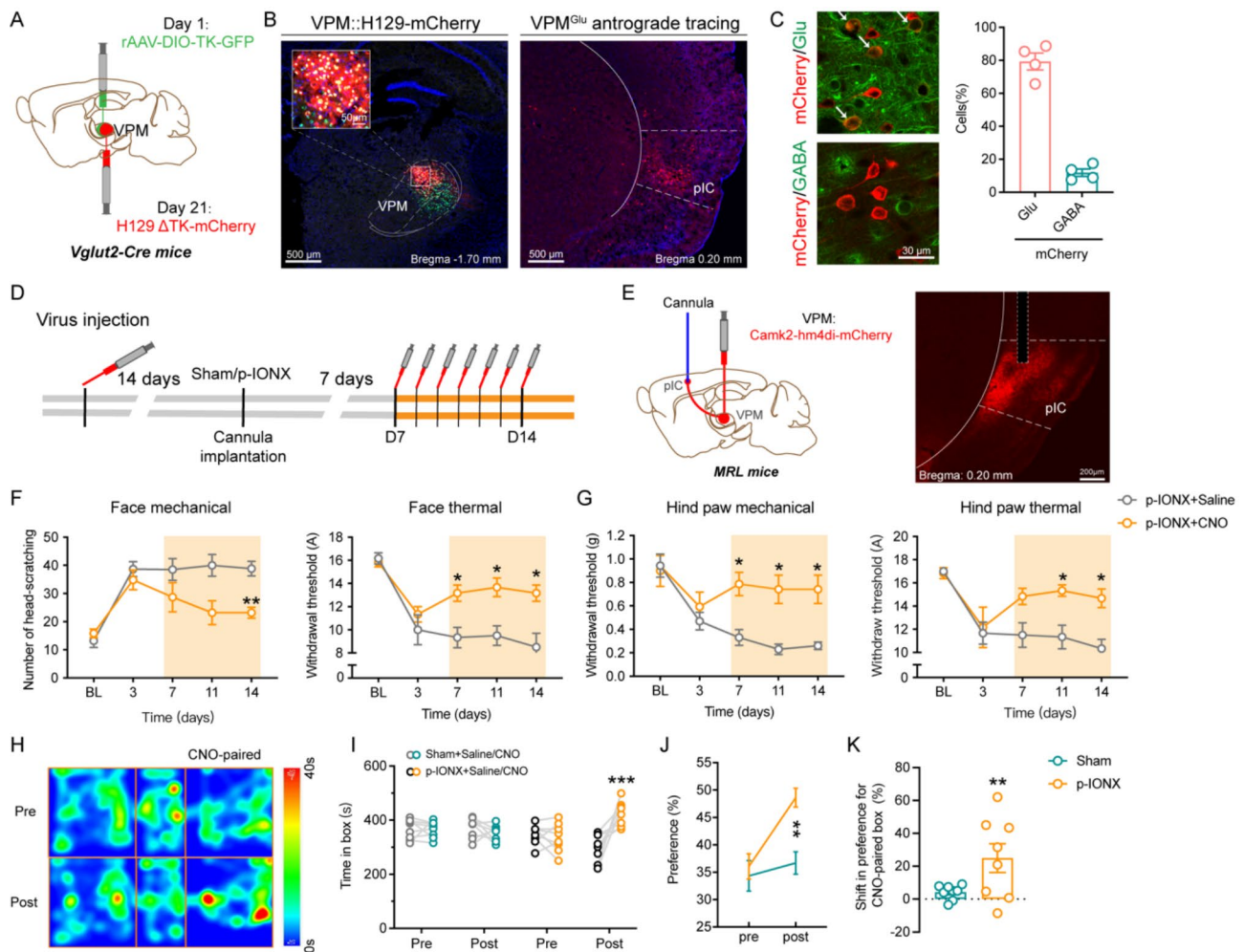


Fig. 5 Chemogenetic inhibition of VPM^{Glu}-pIC circuit alleviates widespread neuropathic pain and associated aversion. **A**, Schematic of the Cre-dependent anterograde trans-monosynaptic herpes simplex virus tracing strategy. **B**, Representative photomicrographs of the virus infection in the VPM of *Vglut2-Cre* mice (left) and m-Cherry-labeled neurons in the pIC (right). Starter cells (yellow) in the left panel co-express AAV-DIO-TK-GFP (green) and h129ΔTK-mCherry (red). The insert depicts the area shown in the white box. **C**, mCherry-labeled neurons within the pIC retrogradely traced from the VPM are co-stained with glutamate (left upper, indicated by white arrows) or GABA (left bottom). Percentage of mCherry-labeled neurons co-expressing glutamate or GABA (right). **D**, Experimental procedure for chemogenetic inhibition of projections of VPM^{Glu} in the pIC. CNO was delivered daily during D7-D14 after p-IONX. **E**, Schematic of CaMKIIα-hm4Di-mCherry injection in the VPM and cannula implantation in the pIC (left) and typical image showing the cannula implantation site (right). **F, G**, Withdrawal thresholds to mechanical and noxious heat stimulation in ipsilateral vibrissal pad (face) and hind paw before and after p-IONX. Yellow shadow areas indicate CNO delivery. **H**, Representative heat maps in the CPP test. **I, J, K**, Time spent by the mice in the saline- and CNO- paired boxes (I), preference (J) and shift preference (K) for the CNO-paired box in pre- and post-conditioning phases. *n* = 8 mice. Significance was calculated by means of two-way ANOVA with Bonferroni's post hoc test in F, G, J; student's *t* test in I, K. **p* < 0.05, ***p* < 0.01 and ****p* < 0.001, p-IONX + Saline versus p-IONX + CNO or post- versus pre- conditioning

trans-monosynaptic retrograde RV spread. We identified intense DsRed-labeled neurons in the ipsilateral barrel field (S1BF), forelimb region (S1FL) and jaw region (S1) of the primary somatosensory cortex, secondary somatosensory cortex (S2), and caudal part of the spinal trigeminal nucleus (Sp5c), etc. Interestingly, the DsRed was evident in the DCN of p-IONX-treated mice, but was hardly observed in the sham-treated group (Fig. 6E-F). We counted the number of neurons in these brain regions projecting to VPM^{Glu} in two groups and found that out of all VPM^{Glu}-projecting neurons, the percentage in the

S1HL, S1Tr, and DCN was significantly increased, while that in the S2 was decreased after p-IONX (Fig. 6G-H). Of note, more projections from the DCN indicate the recruitment of new afferents conveying sensory input from the trunk and limbs.

VPM^{Glu} relay afferents from the DCN to pIC following p-IONX

Tracing experiments were further performed to examine whether the newly recruited afferents of VPM^{Glu} from the DCN after p-IONX were integrated into the pain

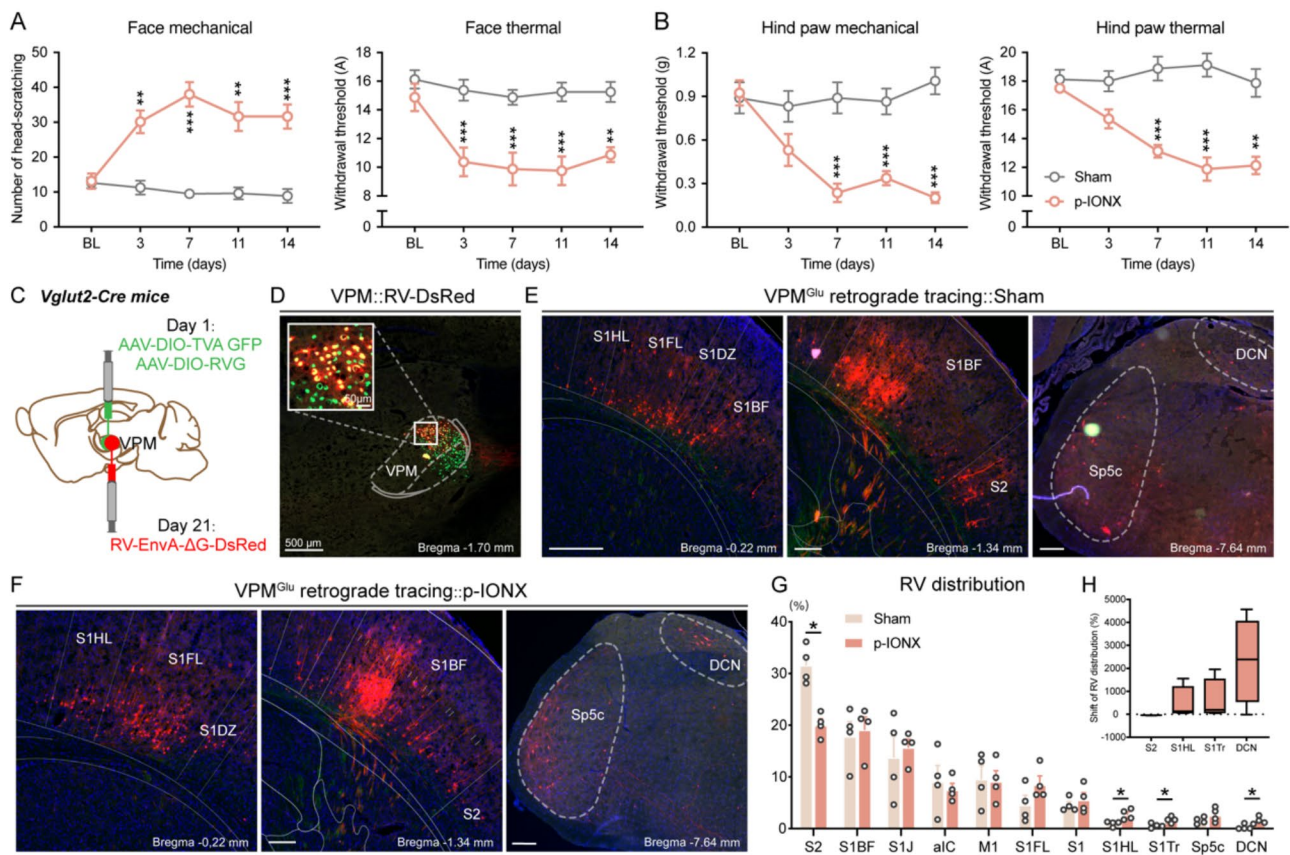


Fig. 6 VPM^{Glu} recruit more afferents from the DCN following p-IONX. **A, B**, Withdrawal thresholds to mechanical and noxious heat stimulation in the ipsilateral vibrissal pad (face, **A**) and hind paw (**B**) before and after p-IONX in *Vglut2-Cre* mice. *n* = 8 mice. **C**, Schematic of the Cre-dependent retrograde trans-monosynaptic tracing strategy. **D**, Typical image of the virus infection site of *Vglut2-Cre* mice. Starter cells (yellow) co-express AAV-DIO-TVA-EGFP, AAV-DIO-RVG (green) and rabies RV-EnvA-ΔG-DsRed (red). The insert depicts the area shown in the white box in the VPM. **E, F**, DsRed-labeled neurons in representative brain regions of sham-**E**) and p-IONX-**F**) treated mice. Scale bar, 500 μm. **G**, Percentage of labeled neurons in each brain region in total retrogradely labeled neurons. aIC, anterior insular cortex; DCN, dorsal column nuclei; M1, primary motor cortex; S1BF, primary somatosensory cortex, barrel field; S1FL, primary somatosensory cortex, forelimb region; S1HL, primary somatosensory cortex, hindlimb region; S1J, primary somatosensory cortex, jaw region; S1Tr, primary somatosensory cortex, trunk region; Sp5c, spinal trigeminal nucleus, caudal part; S2, secondary somatosensory cortex. **H**, Shift of RV distribution ((p-IONX-Sham)/Sham) of the brain regions that significantly changed projection intensity to the VPM. *n* = 4 mice. Significance was calculated by means of two-way ANOVA with Bonferroni's post hoc test in **A, B**. Student's *t* test in **G**. **p* < 0.05, ***p* < 0.01 and ****p* < 0.001, p-IONX versus sham

processing cortex. Cre-dependent virus AAV-CaMKIIα-ChR2-EYFP was injected into the DCN of *Vglut2-Cre* mice on D14 PO, and a mixture of AAV-DIO-TVA-GFP and AAV-DIO-RVG viruses was injected into the pIC. After three weeks of virus expression, RV-ΔG-DsRed was injected into the pIC, followed by one week of expression before perfusion and slicing for observation (Fig. 7A). This approach achieved retrograde trans-monosynaptic tracing of glutamatergic neurons in the pIC (pIC^{Glu}) and anterograde tracing of glutamatergic neurons in the DCN (DCN^{Glu}). The terminals of DCN^{Glu} and the pIC^{Glu}-projecting neurons were labeled with green (EYFP) and red (dsRed) in the thalamus, respectively. Starter cells in the pIC were labeled with both green and red, while DCN^{Glu} with green (Fig. 7B). We found that dsRed-labeled pIC-projecting neurons were distributed in both the VPM and VPL, regardless of the sham and p-IONX groups. Green

projection terminals of DCN were observed almost only in the VPL of sham-treated mice. In the p-IONX group, however, EYFP was observed in both the VPL and VPM. Moreover, there was an overlap of EYFP and dsRed in the VPM of p-IONX mice (Fig. 7C), indicating the VPM might relay the projections from DCN^{Glu} further to pIC^{Glu}.

To provide direct evidence for this speculation, a mixture of AAV-DIO-TVA-mCherry and AAV-DIO-RVG virus was injected into the VPM of *Vglut2-cre* mice, and RV-ΔG-EGFP virus was injected into the pIC 3 weeks later (Fig. 7D). Thus, RV specifically infected pIC^{Glu}-projecting VPM^{Glu} and further trans-monosynaptically labeled the afferent regions with EGFP. We found that in both sham and p-IONX mice, EGFP was distributed in the Sp5c, indicating VPM^{Glu} relay projections of Sp5c neurons to pIC^{Glu}. Moreover, EGFP was also observed

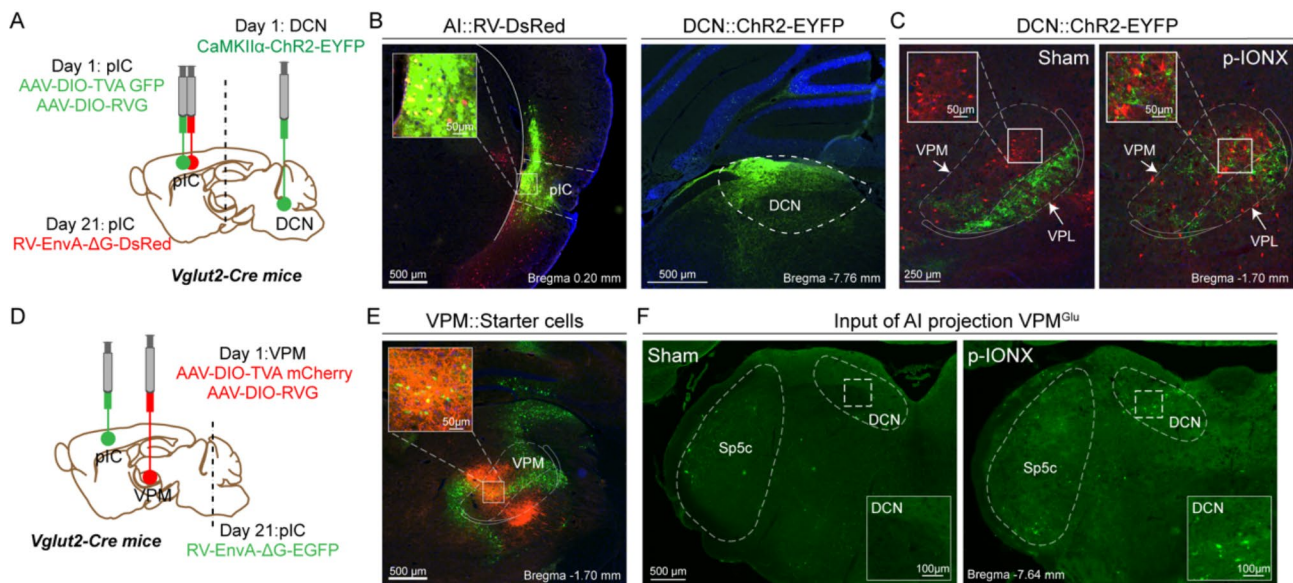


Fig. 7 VPM^{Glu} relay DCN afferents to pIC^{Glu} after p-IONX. **A**, Schematic of the Cre-dependent tracing strategy. **B**, Typical images of the infection site of RV-dsRed in the pIC (left) and AAV-CAG-FLEX-ChR2-EYFP in the DCN (right). **C**, Typical images of dsRed from the pIC and EYFP from the DCN in the VPM and VPL of sham-treated (left) and p-IONX-treated mice (right). **D**, Schematic of the Cre-dependent triple-loop tracing strategy. **E**, Typical image of the starter cells (yellow) in the VPM. **F**, Typical images of EGFP-labeled neurons in the Sp5c and DCN that are retrogradely traced from pIC-projecting VPM^{Glu} in sham-treated (left) and p-IONX-treated mice (right). $n = 4$ mice

in the DCN of p-IONX but not sham group (Fig. 7E-F). These results demonstrate that VPM^{Glu} receive projections from DCN^{Glu} and further project to pIC^{Glu} after p-IONX.

Early inhibition of the DCN-VPM circuit suppresses widespread neuropathic pain

To elucidate the role of the DCN-VPM circuit in the spread of neuropathic pain after p-IONX, we first investigated whether the projections of DCN^{Glu} to VPM after p-IONX were sufficient to activate VPM^{Glu}. We injected AAV-DIO-EGFP in the VPM and AAV-DIO-ChR2-mCherry in the DCN of *Vglut2-Cre* mice to label VPM^{Glu} as green and the terminals of DCN^{Glu} in the VPM as red (Fig. 8A-B). In brain slices, we found that brief blue light stimulation of DCN^{Glu} terminals in the VPM reliably elicited EPSCs in VPM neurons, which were eliminated by the combination of NMDA receptor antagonist AP-5 and AMPA receptor antagonist NBQX (Fig. 8C-D), indicating that VPM^{Glu} recruit new functional sensory input from the DCN after p-IONX. Given that VPM^{Glu} was hyperactive after p-IONX, it is very likely that the increased afferents from the DCN contribute to the spread of neuropathic pain.

This speculation was verified by manipulating the activity of DCN-VPM circuit. AAV-CaMKII α -hM4D(Gi)-mCherry virus was injected into the DCN of MRL mice three weeks before p-IONX, and consecutive inhibition was achieved by administering CNO daily through a cannula implanted in the VPM (Fig. 8E-G). We found that

chemogenetic inhibition of DCN^{Glu} terminals in the VPM during D1-D7 PO relieved orofacial hypersensitization and suppressed the development of pain sensitization in the hind paw. These results demonstrate the necessity of DCN^{Glu}-VPM^{Glu} circuit for p-IONX-induced trigeminal and widespread neuropathic pain. In addition, the analgesic effect gradually vanished after the cease of CNO, as evidenced by thermal and mechanical pain thresholds returning to the levels of saline group on D11 and D14 PO, respectively (Fig. 8H). In contrast, consecutive inhibition of the circuit during D7-D14 PO showed no effect on pain sensitization, both in the face and hind paw (Fig. 8I). These results indicate that the development of widespread pain sensitization after p-IONX is largely dependent on the DCN-VPM circuit, while the maintenance is not, once established.

Discussion

Widespread neuropathic pain, severely impacts patients' physical and mental health and exerts a considerable personal and social burden. The scarcity of effective treatments requires a better understanding of its neuronal basis. One strategy is to achieve a precise recognition of changes in the circuits that are involved in pain transmission after nerve injury. Here, we identified an afferent remodeling of cortex-projecting thalamic neurons induced by infraorbital nerve injury, which gates the spread of neuropathic pain from orofacial to distant body regions. This study not only sheds new light on the mechanisms underlying the spread of pain hypersensitivity

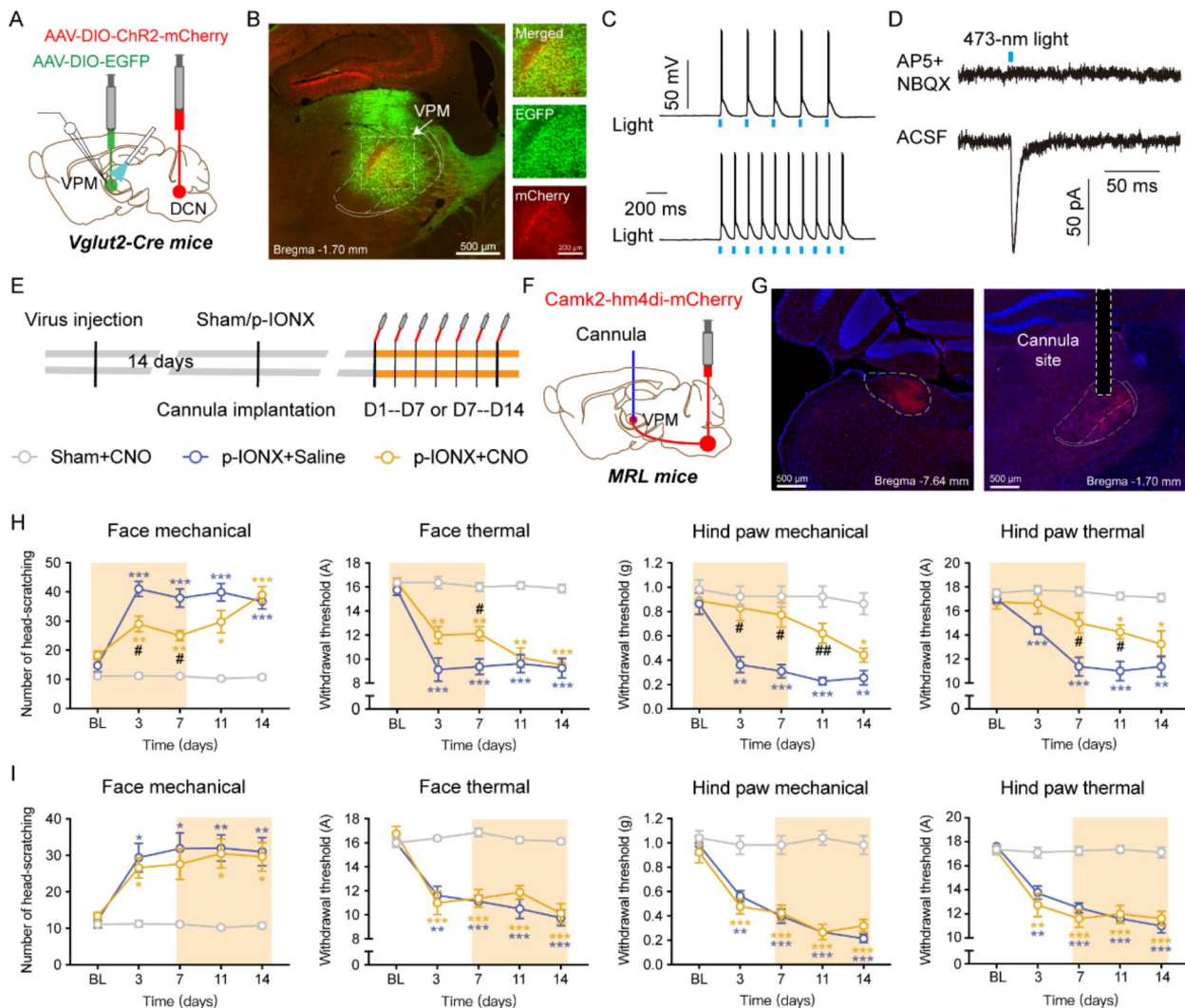


Fig. 8 Early inhibition of DCN-VPM circuit suppresses widespread neuropathic pain. **A**, Schematic of DCN injection of AAV-DIO-ChR2-mCherry and VPM injection of AAV-DIO-EGFP in *Vglut2-Cre* mice and the recording configuration in brain slices. **B**, Typical images of the viral expression in the VPM of *Vglut2-Cre* mice with DCN infusion of AAV-DIO-ChR2-mCherry and VPM infusion of AAV-DIO-EGFP. **C**, Sample traces of action potentials recorded from VPM mCherry⁺ neurons in brain slices with blue light (473 nm, 20 ms, blue bar) stimulation of the DCN terminals in the VPM. **D**, Representative traces of light-evoked currents (473 nm, 20 ms, blue bar) before (lower) and after (upper) AP5 + NBQX (10 μM) treatment. **E**, Experimental design for chemogenetic inhibition of DCN^{Glu} projections in the VPM. CNO was delivered daily during D1–D7 or D7–D14 after p-IONX. **F**, Schematic of the AAV-CamKIIa-hM4D(Gi)-mCherry injection in the DCN and cannula implantation in the VPM of MRL mice. **G**, Typical image of the infection site in the DCN (left) and cannula implantation in the VPM (right). **H, I**, Withdrawal thresholds to mechanical and noxious heat stimulation in the ipsilateral vibrissal pad (face) and hind paw before and after p-IONX. CNO was delivered during D1–D7 after p-IONX, as the yellow shadow shows (H); CNO was delivered daily during D7–D14 after p-IONX, as the yellow shadow shows (I). Significance was calculated by means of one-way ANOVA with Tukey’s post hoc test and two-way ANOVA with Bonferroni’s post hoc test in H, I. *n* = 8 mice. **p* < 0.05, ***p* < 0.01 and ****p* < 0.001, D3, D7, D11 and D14 versus BL in p-IONX + Saline group (blue); D3, D7, D11 and D14 versus baseline in p-IONX + CNO group (yellow); #*p* < 0.05 and ##*p* < 0.01, p-IONX + saline versus p-IONX + CNO

following nerve injury, but also offers new insights into the treatment of widespread neuropathic pain.

The sensory thalamus has long been implicated in neuropathic pain. Following spinal nerve injury, the VPL is consistently engaged in the development of neuropathic pain in the trunk and extremities [38, 39]. By contrast, the VPM is preferentially activated after trigeminal nerve damage and is closely involved in pain in the orofacial area such as TNP, dental pain and migraine [40, 41].

Unsurprisingly, the present study revealed an increase in excitatory neurotransmission and neuronal activity in VPM^{Glu}, but not in VPL^{Glu} after p-IONX. Intriguingly, the shift to hyperactivity of VPM^{Glu} after p-IONX was temporally coinciding with the onset of widespread pain sensitization. Moreover, chemogenetic inhibition of VPM^{Glu} alleviated not only the orofacial pain sensitization, but also the widespread pain sensitization, demonstrating the key role of VPM^{Glu} in TNP and widespread

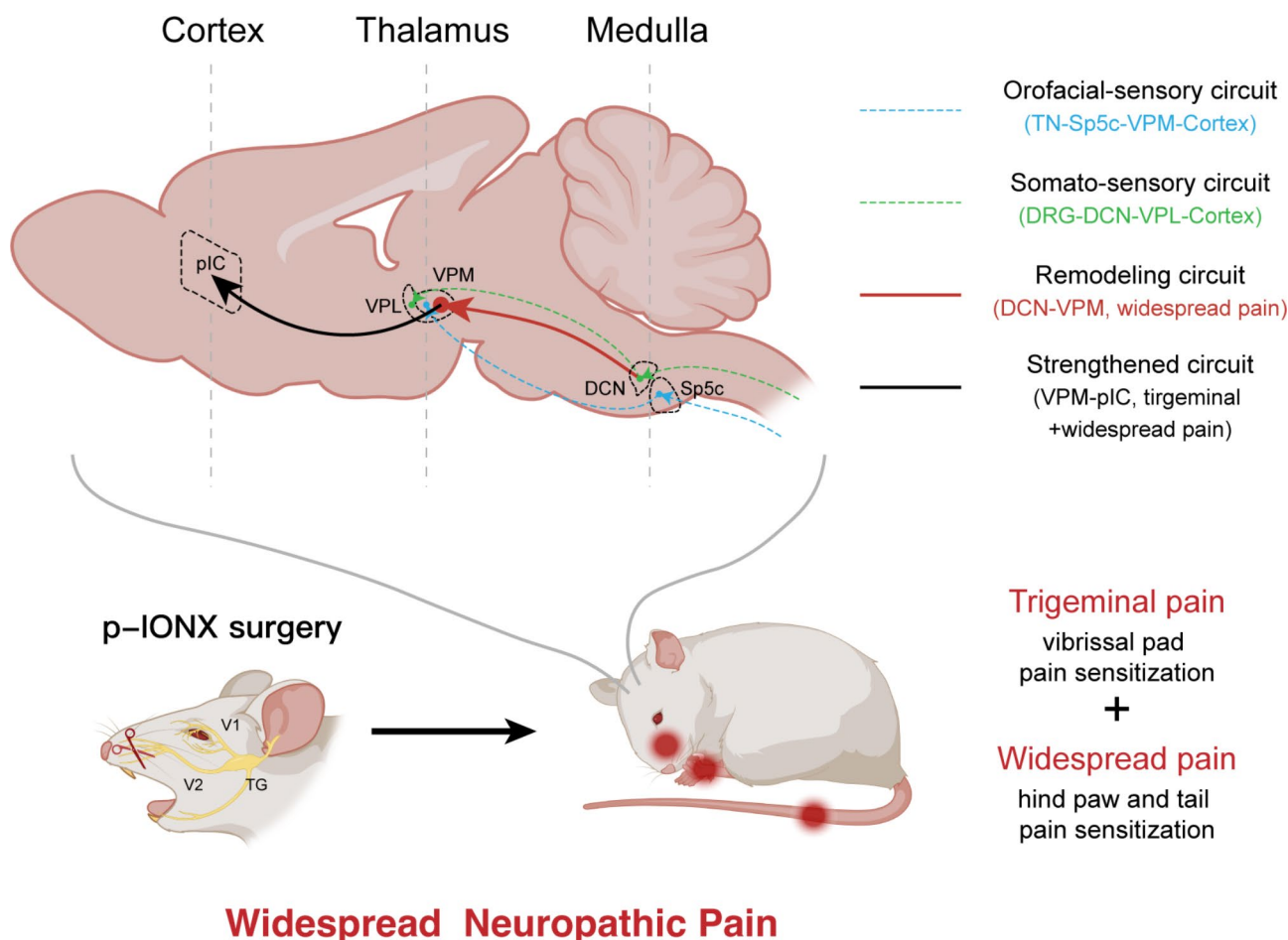


Fig. 9 Graphic abstract of the neural circuit mechanism of widespread neuropathic pain

neuropathic pain. We further elucidated the underlying circuit for the proalgesic role of VPM^{Glu} . It's known that spinothalamic input to relay neurons in sensory thalamus is directed towards the cortex [42]. The circuit to the insula cortex is integral to nociceptive processing, cognitive aspects of pain, and the generation of the pain perception [43, 44]. Particularly, pIC is part of the pain-related cortical networks and plays a fundamental role in the chronicity of pain [45]. We found that chemogenetic inhibition of VPM^{Glu} terminals in the pIC alleviated TNP as well as widespread pain, which is akin to the effect of selective inhibition of VPM^{Glu} . These results demonstrate that hyperactive VPM^{Glu} after p-IONX contribute to trigeminal and widespread neuropathic pain at least via the circuit to pIC. In clinical practice, neuromodulation approaches such as repetitive transcranial magnetic stimulation (rTMS), transcranial direct current stimulation (tDCS) and DBS have been used for refractory neuropathic pain conditions based on their regulation of neuronal excitability [46, 47]. Our study suggests that the VPM^{Glu} -pIC^{Glu} circuit is a potential target of stimulation for the treatment of trigeminal neuropathic pain with or

without spreading and worth further studies in clinical settings.

The transmission of sensory input arising from distant body parts to the pIC via VPM^{Glu} was evidenced by the elevated responsiveness of VPM^{Glu} detected by single-unit and fiber photometry after p-IONX. Additionally, retrograde monosynaptic tracing of VPM^{Glu} revealed a substantial afferent remodeling, manifesting as more afferents from the ipsilateral S1 and contralateral DCN, but less from the ipsilateral S2. Among these, the input from the DCN to VPM^{Glu} showed the most robust change after p-IONX. Furthermore, since the DCN physiologically transmits tactile and proprioceptive information from the trunk and limbs to the contralateral VPL [27], we speculate that the increased afferents from the DCN may underlie the heightened sensitivity of VPM^{Glu} to sensory input from the hind paw or tail. As expected, anterograde tracing experiments revealed that terminals of DCN^{Glu} were distributed in the contralateral VPL in the mice of sham group. However, in p-IONX mice, projections of DCN^{Glu} span both in the VPM and VPL. Moreover, in vitro optogenetic activation

of DCN^{Glu} terminals elicited EPSCs in VPM^{Glu}, indicating VPM^{Glu} recruit more functional afferents from DCN^{Glu}. In addition, triple-loop tracing identified that VPM^{Glu} relay DCN input to pIC^{Glu}, forming a DCN-VPM-pIC pathway. Given the activity of VPM^{Glu} and the circuit to pIC was enhanced following infraorbital nerve injury, the sensory input from the trunk and limbs would activate VPM^{Glu} and further pIC^{Glu}, thus be perceived with hypersensitivity.

The contribution of newly developed DCN-VPM pathway to widespread neuropathic pain was verified by the findings that chemogenetic inhibition of the terminals of DCN^{Glu} in the VPM from D1 to D7 PO suppressed the development of pain hypersensitivity in the hind paw. Interestingly, this treatment also alleviated orofacial pain, indicating a contribution of the excitatory input from the DCN to the hyperexcitability of VPM^{Glu} and trigeminal neuropathic pain. However, inhibiting this circuit from D7 to D14 PO had no effect on pain sensitization either in the hind paw or the face. These results suggest that although the DCN^{Glu}-VPM circuit plays a critical role in the spreading process of neuropathic pain early after trigeminal nerve injury, once the widespread pain sensitization is established, inhibition of this circuit cannot reduce pain either in the orofacial area or distant body parts. This phenomenon is very likely due to that significant sensitization of the VPM and pIC has formed and persists later. These findings suggest that non-invasive stimulation of the pIC and DBS of the VPM may be more effective than stimulating the trunk and limbs for established widespread pain, although the latter may retard the spread of trigeminal pain at early stage. Additionally, following p-IONX, notable changes in projections from upstream nuclei of VPM^{Glu} such as the S2, S1Tr, and S1HL also developed. These regions have been reported to be closely associated with the chronicity of neuropathic pain and thus may also be involved in the maintenance of trigeminal and widespread neuropathic pain [38, 48]. Identification of their exact roles is of great significance for developing new therapeutic strategies. Moreover, whether the excitability of VPL^{Glu} undergoes changes that contribute to widespread pain in later stage requires to be further studied.

Although several lines of evidence indicate that injuries to either spinal or cranial nerve induce remodeling within the neural circuits, the mechanisms underlying this phenomenon are not well understood. During development, CNS neurons demonstrate vigorous axonal growth [49]. However, upon maturation, these neurons lose their intrinsic axonal growth capacity and exhibit diminished reactivation of intrinsic growth programs. Intriguingly, after peripheral nerve damage, synaptic growth capabilities of CNS neurons are rekindled [50, 51]. Multiple factors, including neuron-autonomous

mechanisms, the varied presence of molecular signals and interactions with other cells may be involved in the regulation of axon growth and synapse formation. Emerging evidence underscores the critical role of hypertrophic reactive astrocytes and microglia in inducing local axon sprouting, regulating synaptic plasticity, and orchestrating circuit reorganization [52], [53]. Moreover, neurotrophic factors, such as brain-derived neurotrophic factor (BDNF), neurotrophin-3 (NT3), gliaderived neurotrophic factor (GDNF), etc., are critical for axon regeneration [54]. Indeed, the high expression of inflammatory factors, glial cell activation, and the release of neurotrophic factors are universally present following nerve injury [55, 56]. Our team previously discovered that there is a pervasive onset of neuroinflammation in the brain, including the thalamus, marked by glial activation and the upregulation of proinflammatory cytokines such as HMGB1 following p-IONX [6, 57]. Therefore, neuroinflammatory responses are very likely involved in the afferent remodeling of VPM^{Glu} after p-IONX. However, the distinct patterns of input changes from various brain regions suggest that the reorganization may involve a more complex mechanism.

Conclusion

In summary, the present study reveals that VPM^{Glu} hold a key position in trigeminal and widespread neuropathic pain after infraorbital nerve injury, and the spread of neuropathic pain is related to the remodeling of afferents from the DCN to the VPM. These results not only provide a circuitry explanation for the mechanisms underlying widespread neuropathic pain, but also recommend inhibiting VPM or the glutamatergic circuit to pIC as a potential interventional approach. Future clinical trials to validate the effectiveness and safety of modulating these targets are guaranteed.

Abbreviations

ACSF	Artificial cerebral spinal fluid
ANOVA	Analysis of variance
CPP	Conditioned place preference
CNO	Clozapine N-oxide
DCN	Dorsal column nuclei
DRG	Dorsal root ganglia
ION	Infraorbital nerve
i.p.	Intraperitoneally
pIC	Posterior insular cortex
p-IONX	Partial infraorbital nerve transection
PO	Postoperatively
PWT	Paw withdrawal threshold
sEPSC	Spontaneous excitatory postsynaptic currents
sIPSC	Spontaneous inhibitory postsynaptic currents
TNP	Trigeminal neuropathic pain
VPM	Ventral posteromedial nucleus of the thalamus
VPL	Ventral posterolateral nucleus of the thalamus

Acknowledgements

Not applicable.

Author contributions

SHZ, ZC and WWH designed research; YD, SDL, XQW and YLD performed research; YD, BYX and GDL analyzed data; SHZ, ZC and WWH supervised the experiments. SHZ, ZC and YD wrote the paper.

Funding

This project was supported by grants from the National Natural Science Foundation of China (82073819, 82104136 and 82304459) and partly by Natural Science Foundation of Zhejiang Province (LYY22H310005). Figures 1, 3 and 9 are partly created from BioRender.com and the confirmations of publication and license is provided in supplement.

Data availability

No datasets were generated or analysed during the current study.

Declarations

Ethical approval and consent to participate

All experiments were in accordance with the guidelines of The International Association for the Study of Pain and were approved by the Zhejiang University Animal Care and Use Committee.

Consent for publication

Not applicable.

Competing interests

The authors declare no competing interests.

Received: 16 July 2024 / Accepted: 20 August 2024

Published online: 27 August 2024

References

- Mansfield KE, Sim J, Jordan JL, Jordan KP (2016) A systematic review and meta-analysis of the prevalence of chronic widespread pain in the general population. *Pain* 157:55–64
- Momi SK, Fabiane SM, Lachance G, Livshits G, Williams FMK (2015) Neuropathic pain as part of chronic widespread pain: environmental and genetic influences. *Pain* 156:2100–2106
- McBeth J, Mulvey MR, Rashid A, Anderson J, Druce K (2019) The relationship between regional pain with or without neuropathic symptoms and chronic widespread pain. *Pain* 160:1817–1823
- Okada-Ogawa A et al (2015) Involvement of medullary GABAergic system in extraterritorial neuropathic pain mechanisms associated with inferior alveolar nerve transection. *Exp Neurol* 267:42–52
- Yu N et al (2024) IL-6 from cerebrospinal fluid causes widespread pain via STAT3-mediated astrocytosis in chronic constriction injury of the infraorbital nerve. *J Neuroinflammation* 21:60
- Zhang SH et al (2016) Widespread pain sensitization after partial infraorbital nerve transection in MRL/MPJ mice. *Pain* 157:740–749
- Cruccu G, Di Stefano G, Truini A (2020) Trigeminal neuralgia. *N Engl J Med* 383:754–762
- Türp JC, Kowalski CJ, O'Leary N, Stohler CS (1998) Pain maps from facial pain patients indicate a broad pain geography. *J Dent Res* 77:1465–1472
- Bendtsen L et al (2020) Advances in diagnosis, classification, pathophysiology, and management of trigeminal neuralgia. *Lancet Neurol* 19:784–796
- Hu TT et al (2018) TLR4 deficiency abrogated widespread tactile allodynia, but not widespread thermal hyperalgesia and trigeminal neuropathic pain after partial infraorbital nerve transection. *Pain* 159:273–283
- Hu TT et al (2020) A crucial role of HMGB1 in orofacial and widespread pain sensitization following partial infraorbital nerve transection. *Brain Behav Immun* 88:114–124
- Navarro X, Vivó M, Valero-Cabré A (2007) Neural plasticity after peripheral nerve injury and regeneration. *Prog Neurobiol* 82:163–201
- Jain N, Qi HX, Collins CE, Kaas JH (2008) Large-scale reorganization in the somatosensory cortex and thalamus after sensory loss in macaque monkeys. *J Neurosci* 28:11042–11060
- Kim SK, Nabekura J (2011) Rapid synaptic remodeling in the adult somatosensory cortex following peripheral nerve injury and its association with neuropathic pain. *J Neurosci* 31:5477–5482
- Yamahachi H, Marik SA, McManus JN, Denk W, Gilbert CD (2009) Rapid axonal sprouting and pruning accompany functional reorganization in primary visual cortex. *Neuron* 64:719–729
- Flor H, Nikolajsen L, Staehelin Jensen T (2006) Phantom limb pain: a case of maladaptive CNS plasticity? *Nat Rev Neurosci* 7:873–881
- Kambi N et al (2014) Large-scale reorganization of the somatosensory cortex following spinal cord injuries is due to brainstem plasticity. *Nat Commun* 5:3602
- Chand P, Jain N (2015) Intracortical and thalamocortical connections of the Hand and face representations in Somatosensory Area 3b of Macaque monkeys and effects of chronic spinal cord injuries. *J Neurosci* 35:13475–13486
- Vartiainen N et al (2016) Thalamic pain: anatomical and physiological indices of prediction. *Brain* 139:708–722
- Kramer PR et al (2017) Role for the ventral posterior Medial/Posterior lateral thalamus and Anterior Cingulate Cortex in Affective/Motivation Pain Induced by Varicella Zoster Virus. *Front Integr Neurosci* 11:27
- Blomqvist A, Zhang ET, Craig AD (2000) Cytoarchitectonic and immunohistochemical characterization of a specific pain and temperature relay, the posterior portion of the ventral medial nucleus, in the human thalamus. *Brain* 123 Pt 3:601–619
- Arvidsson J, Rice FL (1991) Central projections of primary sensory neurons innervating different parts of the vibrissae follicles and intervibrissal skin on the mystacial pad of the rat. *J Comp Neurol* 309:1–16
- Willis WD, Al-Chaer ED, Quast MJ, Westlund KN (1999) A visceral pain pathway in the dorsal column of the spinal cord. *Proc Natl Acad Sci U S A* 96:7675–7679
- Elina KC, Oh BH, Islam J, Kim S, Park YS (2021) Activation of CamKII α expressing neurons on ventrolateral periaqueductal gray improves behavioral hypersensitivity and thalamic discharge in a trigeminal neuralgia rat model. *J Headache Pain* 22:47
- Ben-Haim S, Mirzadeh Z, Rosenberg WS (2018) Deep brain stimulation for intractable neuropathic facial pain. *Neurosurg Focus* 45:E15
- Takeuchi Y, Yamasaki M, Nagumo Y, Imoto K, Watanabe M, Miyata M (2012) Rewiring of afferent fibers in the somatosensory thalamus of mice caused by peripheral sensory nerve transection. *J Neurosci* 32:6917–6930
- Takeuchi Y, Osaki H, Yagasaki Y, Katayama Y, Miyata M (2017) Afferent Fiber Remodeling in the Somatosensory Thalamus of Mice as a Neural Basis of Somatosensory Reorganization in the Brain and Ectopic Mechanical Hypersensitivity after Peripheral Sensory Nerve Injury. *eNeuro* 4
- Zimmermann M (1983) Ethical guidelines for investigations of experimental pain in conscious animals. *Pain* 16:109–110
- Wang Y et al (2018) Increased Asics expression via the Camkii-CREB pathway in a Novel Mouse Model of Trigeminal Pain. *Cell Physiol Biochem* 46:568–578
- Bonin RP, Bories C, De Koninck Y (2014) A simplified up-down method (SUDO) for measuring mechanical nociception in rodents using Von Frey filaments. *Mol Pain* 10:26
- King T et al (2009) Unmasking the tonic-aversive state in neuropathic pain. *Nat Neurosci* 12:1364–1366
- Wang Y et al (2017) Depolarized GABAergic Signaling in Subicular Microcircuits mediates generalized seizure in temporal lobe Epilepsy. *Neuron* 95:92–105e105
- Csicsvari J, Hirase H, Czurkó A, Mamiya A, Buzsáki G (1999) Oscillatory coupling of hippocampal pyramidal cells and interneurons in the behaving rat. *J Neurosci* 19:274–287
- Le Van Quyen M, Bragin A, Staba R, Crépon B, Wilson CL, Engel J (2008) Jr. Cell type-specific firing during ripple oscillations in the hippocampal formation of humans. *J Neurosci* 28:6104–6110
- Roy DS, Zhang Y, Halassa MM, Feng G (2022) Thalamic subnetworks as units of function. *Nat Neurosci* 25:140–153
- Gu X et al (2012) Anterior insular cortex is necessary for empathetic pain perception. *Brain* 135:2726–2735
- Labrakakis C (2023) The role of the Insular Cortex in Pain. *Int J Mol Sci* 24
- Guo F et al (2023) Secondary somatosensory cortex glutamatergic innervation of the thalamus facilitates pain. *Pain*
- Miki K et al (2000) Dorsal column-thalamic pathway is involved in thalamic hyperexcitability following peripheral nerve injury: a lesion study in rats with experimental mononeuropathy. *Pain* 85:263–271
- Krüger MT et al (2021) Directional deep brain stimulation can target the thalamic Sweet Spot for improving Neuropathic Dental Pain. *Oper Neurosurg (Hagerstown)* 21:81–86

41. Lim M, Jassar H, Kim DJ, Nascimento TD, DaSilva AF (2021) Differential alteration of fMRI signal variability in the ascending trigeminal somatosensory and pain modulatory pathways in migraine. *J Headache Pain* 22:4
42. Dum RP, Levinthal DJ, Strick PL (2009) The spinothalamic system targets motor and sensory areas in the cerebral cortex of monkeys. *J Neurosci* 29:14223–14235
43. Segerdahl AR, Mezue M, Okell TW, Farrar JT, Tracey I (2015) The dorsal posterior insula subserves a fundamental role in human pain. *Nat Neurosci* 18:499–500
44. Stancak A, Fallon N (2013) Emotional modulation of experimental pain: a source imaging study of laser evoked potentials. *Front Hum Neurosci* 7:552
45. Lu C et al (2016) Insular Cortex is critical for the Perception, Modulation, and Chronification of Pain. *Neurosci Bull* 32:191–201
46. Hoogendam JM, Ramakers GM, Di Lazzaro V (2010) Physiology of repetitive transcranial magnetic stimulation of the human brain. *Brain Stimul* 3:95–118
47. Stagg CJ, Antal A, Nitsche MA (2018) Physiology of Transcranial Direct Current Stimulation. *J ect* 34:144–152
48. Wrigley PJ et al (2009) Neuropathic pain and primary somatosensory cortex reorganization following spinal cord injury. *Pain* 141:52–59
49. Goldberg JL (2003) How does an axon grow? *Genes Dev* 17:941–958
50. He Z, Jin Y (2016) Intrinsic control of Axon Regeneration. *Neuron* 90:437–451
51. Bradke F, Fawcett JW, Spira ME (2012) Assembly of a new growth cone after axotomy: the precursor to axon regeneration. *Nat Rev Neurosci* 13:183–193
52. Anderson MA et al (2016) Astrocyte scar formation aids central nervous system axon regeneration. *Nature* 532:195–200
53. Yang Z, Suzuki R, Daniels SB, Brunquell CB, Sala CJ, Nishiyama A (2006) NG2 glial cells provide a favorable substrate for growing axons. *J Neurosci* 26:3829–3839
54. Gomez N, Lu Y, Chen S, Schmidt CE (2007) Immobilized nerve growth factor and microtopography have distinct effects on polarization versus axon elongation in hippocampal cells in culture. *Biomaterials* 28:271–284
55. Ji RR, Chamesian A, Zhang YQ (2016) Pain regulation by non-neuronal cells and inflammation. *Science* 354:572–577
56. Inoue K, Tsuda M (2018) Microglia in neuropathic pain: cellular and molecular mechanisms and therapeutic potential. *Nat Rev Neurosci* 19:138–152
57. Du Y et al (2022) HMGB1 in the mPFC governs comorbid anxiety in neuropathic pain. *J Headache Pain* 23:102

Publisher's note

Springer Nature remains neutral with regard to jurisdictional claims in published maps and institutional affiliations.